

Morphological estimation of primary branch length of individual apple trees during the deciduous period in modern orchard based on PointNet++

Xiaoming Sun^a, Leilei He^a, Hanhui Jiang^a, Rui Li^{a,*}, Wulan Mao^{a,e}, Dong Zhang^f, Yaqoob Majeed^g, Nikita Andriyanov^h, Vladimir Soloviev^h, Longsheng Fu^{a,b,c,d,*}

^a College of Mechanical and Electronic Engineering, Northwest A&F University, Yangling, Shaanxi, 712100, China

^b Key Laboratory of Agricultural Internet of Things, Ministry of Agriculture and Rural Affairs, Yangling, Shaanxi 712100, China

^c Shaanxi Key Laboratory of Agricultural Information Perception and Intelligent Service, Yangling, Shaanxi 712100, China

^d Northwest A&F University Shenzhen Research Institute, Shenzhen, Guangdong 518000, China

^e Institute of Agricultural Mechanization, Xinjiang Academy of Agricultural Sciences, Urumqi 830000, China

^f College of Horticulture, Northwest A&F University, Yangling, Shaanxi, 712100, China

^g Faculty of Agricultural Engineering and Technology, University of Agriculture, Faisalabad 38000, Pakistan

^h Department of Data Analysis and Machine Learning, Financial University under the Government of the Russian Federation, Moscow 125167, Russia



ARTICLE INFO

Keywords:

Morphological trait
Primary branch instance
Point cloud
Deep learning
Part segmentation

ABSTRACT

Primary branch length is an important morphological trait of individual apple tree phenotypes. This study presents a novel method for estimating the primary branch lengths of individual apple trees during the deciduous period by distinguishing their instances, i.e., merging those belonging to the same primary branch based on part segmentation outputs of PointNet++. Firstly, colored and colorless 3D-datasets were prepared for training PointNet++ models. The model with higher overall accuracy (OA), class average accuracy (CAA), and mean intersection-over-union ($mIoU$) was employed to segment the point cloud of a tree into primary branches (PB), trunk (TK), and end-points of primary branches (EPB) of individual apple trees. Skeletonization was applied to the outputs of the three parts of individual apple trees. Subsequently, each primary branch instance was distinguished by determining its corresponding path and retaining the longest path of the same primary branch only. Finally, the primary branch length was estimated by calculating the sum of Euclidean distances between adjacent points on the corresponding path. Results indicated that adding color to point clouds did not improve segmentation accuracy of PointNet++ on segmenting PB, TK, and EPB with similar color features. The PointNet++ model that was trained without color achieved an OA, CAA, and $mIoU$ of 0.84, 0.83, and 0.70, respectively. The proportion of estimated and ground-truth values of the number of primary branches was 93.64 %. The mean absolute percentage error of estimating primary branch lengths was 12.00 %. These findings demonstrate that the proposed method is promising for high-throughput phenotyping of apple trees.

1. Introduction

Primary branch length is a crucial morphological trait of individual apple tree phenotypes. Primary branches of an apple tree originate directly from the trunk, which reflect the main structure of tree canopy (Akter et al., 2021; Liu et al., 2023; Wu et al., 2020; Zhang et al., 2020). Their lengths serve as a key indicator for the assessment of apple tree vigor (Zine-El-Abidine et al., 2021). Measuring the primary branch lengths also contributes to obtaining a well-balanced canopy structure through branch pruning (Chen et al., 2021; Kok et al., 2023; Miao et al., 2021; Zhang et al., 2018). Consequently, it is important to measure the

primary branch lengths for apple tree phenotypes.

Manual measurement of the primary branch lengths of an individual apple tree is typically performed by fruit growers using soft rulers. However, completing the measurement of apple tree phenotypes for the entire orchard within a limited time frame is a laborious task, especially when dealing with curved and crisscrossed primary branches (Sun et al., 2022; Suo et al., 2022; Zahid et al., 2021; Zhao et al., 2023). Therefore, there is an increasing need for automatic estimation of the primary branch lengths of apple trees in modern orchards.

Some researchers have focused on dormant trees for estimating various branch traits such as lengths, diameters, and number of

* Corresponding authors at: College of Mechanical and Electronic Engineering, Northwest A&F University, Yangling, Shaanxi, 712100, China (R. Li and L. Fu).
E-mail addresses: ruili1216@nwafu.edu.cn (R. Li), fulsh@nwafu.edu.cn (L. Fu).

branches. For example, Akbar et al. (2016) measured the primary branch diameters of dormant apple trees based on a linear model between estimated diameters and depth values, which reached an accuracy of 89 %. Zhang et al. (2023) employed a hierarchical growing method to extract the primary branch lengths of apple trees with a mean absolute error of 0.025 m during the dormant stage. Although there was a large literature on the characterization of tree architecture through skeletonization, only the skeleton of the whole apple tree can be obtained (Wu et al., 2021). Primary branch instances were not distinguished one by one, hence their lengths were not estimated (Fan et al., 2020). Moreover, previous approaches mainly targeted dormant apple trees with simpler canopy structures than those during the deciduous period (Bucksch and Fleck, 2011).

Other than the dormant period, there is a need for automatically estimating primary branch traits of apple trees during different periods for various field operation tasks such as vibratory harvesting of apples and spraying of apple tree canopy. During the deciduous period, curled leaves are still present on curved and crisscross primary branches, which poses a challenge in distinguishing branch instances and estimate their traits (Abdel-Sattar and Kotb, 2021; Jiang et al., 2023; Zhang et al., 2021a). Contrarily to already published studies that focus on phenotyping of apple trees only during the dormant period, the research goal of this study is to estimate branch traits during the deciduous period.

Distinguishing primary branch instances is essential for automatically estimating branch traits of apple trees during the deciduous period. Some researchers have distinguished branch instances directly from RGB (Red, Green, and Blue) images of trees using instance segmentation networks (Feng et al., 2022; Liang et al., 2022). Yang et al. (2019) and Tong et al. (2022) employed Mask Region-based Convolutional Neural Network (Mask R-CNN) to distinguish each branch instance of citrus and apple trees in RGB images, which achieved average precision (*AP*) values of 0.98 and 0.94, respectively. Similarly, Borrenpohl and Karkee (2023) applied Mask R-CNN to distinguish upright branch instances of dormant sweet cherry trees from RGB images captured under active lighting with an intersection-over-union (*IoU*) of 0.78. Although these studies successfully distinguished each branch instance of trees using RGB images, they didn't estimate branch lengths directly due to the lack of three-dimensional (3D) information (Wang et al., 2022a).

Point clouds with 3D information have been utilized to distinguish each primary branch instance using machine learning techniques. Machine learning is a prevalent method to distinguish each primary branch instance in point clouds (Straub et al., 2022). Qiu et al. (2022) used density-based spatial clustering of applications with noise (DBSCAN) method to group leafless branches based on point clouds of individual apple trees. Itakura et al. (2022) segmented each branch instance of trees of various species using a region-growing algorithm in point clouds after classifying leaf and branch points with an overall classification accuracy of 94.83 %. However, it was difficult to correctly distinguish each primary branch instance of trees during the deciduous period from point clouds using machine learning due to missing of some primary branch points and low correlation between color and depth.

Point cloud segmentation based on deep learning has been applied to segment complex and occluded point clouds robustly. Point cloud segmentation can be categorized into instance segmentation and semantic segmentation. For instance segmentation, Wang et al. (2022b) proposed PartNet to segment each instance of lettuce leaves from a point cloud synthesized using eight perspective images, which reported an *AP* of 0.92 at 0.5 of *IoU*. However, the task of instance segmentation for complex and occluded point clouds still presents significant challenges and limitations in distinguishing their instances directly.

Therefore, previous studies have also explored semantic segmentation of complex and occluded point clouds. For example, Qi et al. (2017) proposed PointNet++ (a classification or segmentation network for point clouds) that can learn features from the point set efficiently and robustly. For segmentation of point clouds, PointNet++ targeted part segmentation for single objects and semantic segmentation for scenes

including multiple objects. Additionally, some researchers added color or vector information to improve the segmentation accuracy of PointNet++ (Wang et al., 2020; Zhou et al., 2021). Although it shows promise in segmenting individual apple trees into different parts, including primary branches, during the deciduous period, further processing is required to distinguish each primary branch instance based on part segmentation outputs and estimate their traits.

In this study, a novel method of estimating the primary branch length of apple trees during the deciduous period was proposed, which distinguished each primary branch instance based on part segmentation outputs obtained by PointNet++. In this study, two PointNet++ models were trained separately on point clouds of individual apple trees with and without color information. Then the PointNet++ model with higher segmentation accuracy was employed to segment the point cloud of a tree into primary branches (PB), trunk (TK), and end-points of primary branches (EPB). At the end, each primary branch instance was distinguished by determining its corresponding path to estimate its length. The remaining of this paper is organized as follows. Section 2 illustrates a novel method for estimating the primary branch length based on PointNet++. In Section 3, results and discussion are given. Lastly, conclusions of this study are summarized in Section 4.

2. Materials and methods

2.1. Data acquisition

A data acquisition system was developed to collect point clouds and corresponding RGB images of the entire individual apple trees during the deciduous period from a single perspective. It mainly consisted of a light detection and ranging (LiDAR) (Mid-70, Livox, Shenzhen, China), an RGB camera (MV-CA050-20UC, HikRobot, Hangzhou, China), and a tripod, which had a vertical height of about 1.4 m, as shown in Fig. 1. Mid-70 (a LiDAR), had a random error of 0.02 m within a 20 m range and a circular field of view of 70.4°. RGB images were acquired by using MV-CA050-20UC camera, whose resolution was 2,592 × 2,048 pixels. The RGB camera was fixed on top of the selected LiDAR using a 3D printed connector. Then, the combined RGB camera and LiDAR were mounted on a tripod.

All data were collected by the data acquisition system in a modern orchard located in Wuquan (34°18' N, 108°0' E), Shaanxi Province, China. In this orchard, several varieties of three years old apple trees were planted with a tree spacing of 1.5 m and a row spacing of 3.3 m. The distance between a target apple tree and the data acquisition system was set to be about 3.0 m during the collection process. At the same time, the target individual apple tree during the deciduous period was kept in the center. In total, 122 pairs of point clouds and corresponding RGB images were randomly collected in the orchard using the data acquisition system. The original data are available on https://github.com/fu3lab/Apple_tree_pointclouds.

For each apple tree, three primary branches were randomly selected to manually measure their lengths using a soft ruler. Some of the randomly selected apple trees have only two primary branches. In that case, the lengths of them were also manually measured. The selected primary branches were marked with stickers to make them visible in the corresponding RGB image, as shown in Fig. 2. The average value of three repeated manual measurements of each primary branch length was regarded as the ground truth. The number of primary branches on each apple tree was also recorded.

2.2. Data preprocessing

2.2.1. Format conversion of point clouds

Raw point clouds from Mid-70 were initially collected in the 'LVX' format, which were subsequently converted into the 'PCD' (Point Cloud Data) format for further processing. Each raw point cloud in the 'LVX' format was parsed and organized into multiple point clouds in the 'PCD'



Fig. 1. Schematics of front view (a) and side view (b) of data acquisition system.



Fig. 2. Example of an RGB image of apple trees during the deciduous period. Red rectangles show the selected primary branches marked by stickers.

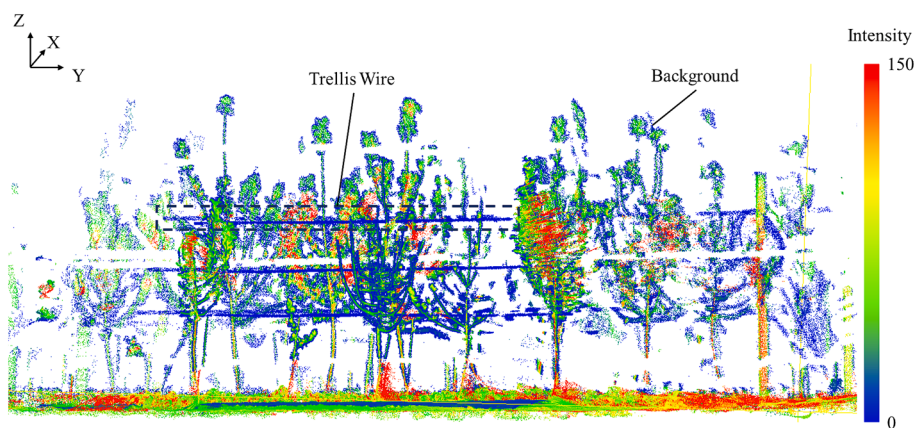


Fig. 3. Example of a point cloud in the 'PCD' format displayed in the Cloud Compare (an open-source software, <http://www.cloudcompare.org>). Colors of points are rendered from blue to red as their intensity increased from 0 to 150 for diffuse objects. Blue points in the black dashed box are trellis wire points while the background includes apple trees in the back rows.

format based on their timestamps. These point clouds in the ‘PCD’ format were then merged into a single point cloud.

Point clouds in the ‘PCD’ format consisted of five channels, representing X, Y, and Z coordinates, intensity information, and tag information. Other than the target apple tree points, each point cloud also contained some trellis wires and background points. Example of a point cloud in the ‘PCD’ format is shown in Fig. 3. X, Y, and Z coordinates represent depth, width, and height information, respectively, and are defined relative to Mid-70. Intensity information provides reflective intensity values ranging from 0 to 150 (0 for objects with a reflectivity of 0 % and 150 for objects with a reflectivity of 100 %) for diffuse reflective objects. Tag information recorded multiple echoes and noise information. In this study, all points were normal points returned by the first echo.

2.2.2. Removing trellis wires and background

To obtain point clouds of individual apple trees, trellis wires and background were removed, as shown in Fig. 4(a). Trellis wires were removed from the point clouds using intensity information because their reflectivity was different from that of apple trees. To remove trellis wires, an intensity threshold value of 5 was used. This threshold value was selected based on manual observation. All points with intensity value less than and equal to 5 were replaced with 0. Further background points were removed based on X coordinate, i.e., depth information. Any points beyond this range were considered part of the background and then removed since the depth of the target apple tree was about 3.0 m during data collection. Then, the point clouds of individual apple trees were manually segmented using the Cloud Compare software, as shown in Fig. 4(b). After that, each segmented point cloud only contained coordinate information of a single apple tree, i.e., X, Y, and Z coordinates, without retaining intensity and tag information.

2.3. Part segmentation of point clouds

2.3.1. Generating colored point clouds

After obtaining colorless point clouds of individual apple trees, PB, TK, and EPB needed to be segmented by PointNet++. To verify whether adding color information can improve part segmentation accuracy of PointNet++, colored and colorless point clouds needed to be annotated to make two 3D datasets that were named as colored 3D-dataset and colorless 3D-dataset, respectively. Colored point clouds were generated to the colored 3D-dataset by mapping RGB information onto the original colorless point cloud.

Internal parameters of the RGB camera and external parameters between it and the LiDAR were calibrated to map RGB information onto the original colorless point cloud. Internal parameters of the RGB camera were calibrated using Zhang’s calibration method (Liu et al., 2024; Zhang, 1999). External parameters between the RGB camera and the

LiDAR were calibrated using an open-source algorithm provided by Livox (https://github.com/Livox-SDK/livox_camera_lidar_calibration). Point clouds and corresponding RGB images of a calibration board with low reflectivity were collected at different angles and distances using the data acquisition system, as shown in Fig. 5(a). Then, 3D coordinates and corresponding pixel coordinates of four corner points of the calibration board were manually determined to obtain calibrated external parameters. Finally, colored point clouds were generated. The upper points of some colored point clouds of individual apple trees were mapped as white due to over exposure, as shown in Fig. 5(b). It is worth noting that there were some gaps in the point clouds of individual apple trees, mainly caused by occlusion from primary branches and leaves, as shown in Fig. 5(c).

2.3.2. Dataset annotation

The colored and colorless 3D-datasets were separately annotated for contrasting the part segmentation accuracy of training PointNet++ with and without color information. Firstly, colorless point clouds of individual apple trees were labeled with three classes, i.e., PB, TK, and EPB. The annotation of colorless point clouds was carried out using the Cloud Compare software by assigning scalar fields of 0, 1, and 2 to the respective classes, as shown in Fig. 6. EPB referred to the part of primary branch away from the trunk. The points on the primary branch with distances to the trunk greater than a threshold were labeled as EPB. A value greater than the median distances of all points of the primary branch to the trunk was selected as the threshold. The points with distances less than this threshold were labeled as PB which connected directly to the trunk. The point clouds were annotated and saved in ‘TXT’ format to make a suitable colorless 3D-dataset. Then, corresponding annotation files with color were generated by adding color information to the annotation files of the colorless point clouds. For both colored and colorless 3D-datasets, 70 % of the annotation files of the point clouds (85 annotated point clouds) were randomly assigned as the training set while the remaining annotation files of the point clouds (37 annotated point clouds) were reserved for the testing set.

2.3.3. Preprocessing for part segmentation of PointNet++

The point clouds were preprocessed before input into the PointNet++ network for part segmentation. Data preprocessing included down-sampling and normalization. Firstly, number of points in raw point clouds ranged from 8,564 to 448,464. Raw point clouds with more than 20,000 points were randomly and uniformly down-sampled to 20,000. Then, to improve the accuracy of PointNet++, the point clouds were normalized by scaling the 3D coordinates to the range of -1 to 1. After down-sampling, the point clouds were processed by PointNet++ network for part segmentation.

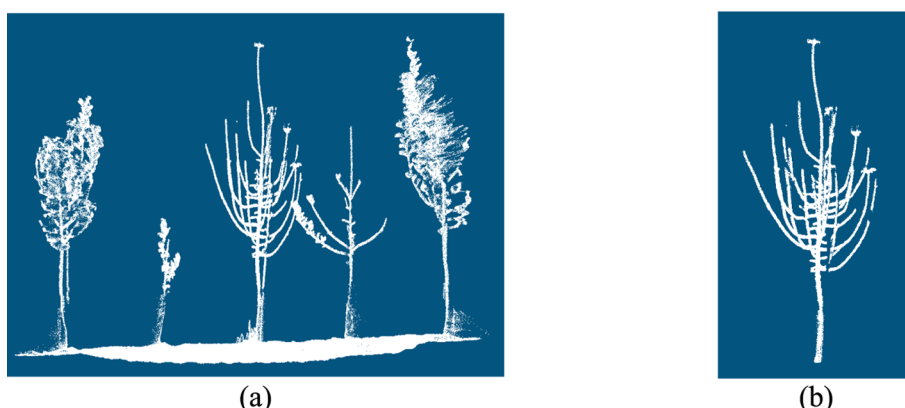


Fig. 4. Example of a point cloud with trellis wires and background points removed (a) and an individual apple tree (b).

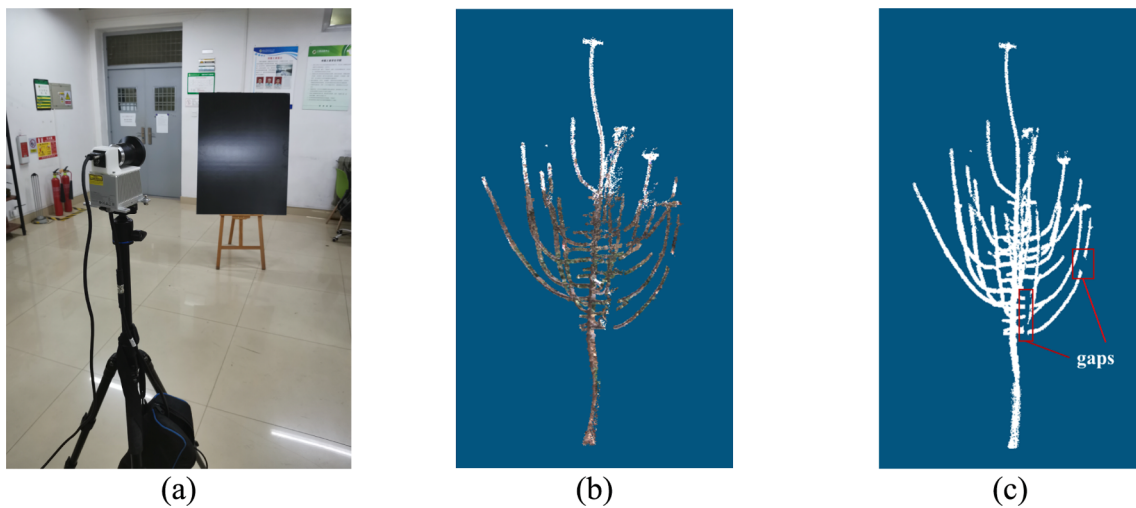


Fig. 5. Example of collecting point clouds and RGB images of the calibration board (a). A colored point cloud of an individual apple tree (b). Some gaps in the colorless point cloud (c).

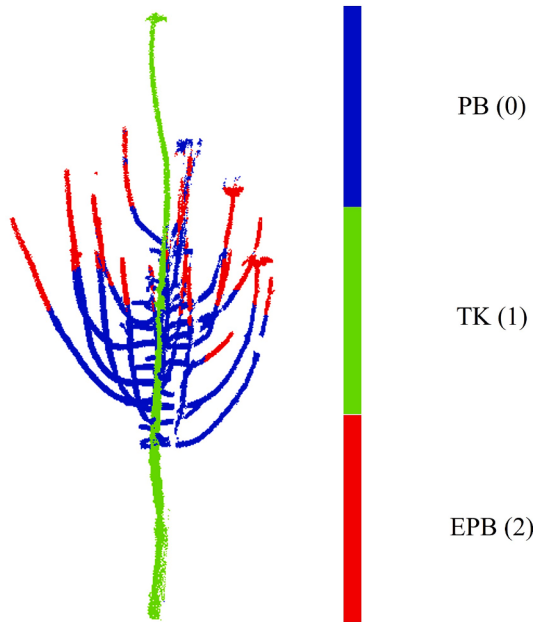


Fig. 6. Example of a point cloud of an individual apple tree that was labeled with three classes, i.e., PB, TK, and EPB using the Cloud Compare software. Points of PB, TK, and EPB are painted as blue, green, and red, respectively.

2.3.4. Training PointNet++ models with and without color

Two PointNet++ models, one trained with color (PWC) and the other trained without color (PNC) were trained separately to segment the PB, TK, and EPB of individual apple trees. They were trained on a laptop computer equipped with a Nvidia GeForce GTX 3050Ti 4 GB GPU and 16 GB of memory based on Windows operating system (https://github.com/yanx27/Pointnet_Pointnet2_pytorch). The same training parameters were set to train both PWC and PNC. Learning rate, batch size, and number of epochs were set as 0.01, 4, and 250, respectively. The optimal PointNet++ model was utilized to estimate the primary branch length.

2.4. Estimation of primary branch length

2.4.1. Skeletonization

To reduce irrelevant points and improve the speed of estimating the

primary branch length, points of the PB, TK, and EPB of individual apple trees were separated and then skeletonized independently. Using the optimal PointNet++ model, prediction files of the testing set were generated. Scales of the point clouds were restored to their original scales, and were stored in the format of 'PCD'. Three parts of individual apple trees were separated based on the prediction values of the optimal PointNet++ model, as shown in Fig. 7(b). Outlier points were removed based on radius filtering, where points with less than six neighbors within a radius of 0.05 m were removed. Then, each part was skeletonized using Lee's method based on two considerations (Lee et al., 1994), as shown in Fig. 7(c). Core skeleton was only kept while outer edge points were discarded, ensuring that the essential structure of each part was preserved. The skeletonization operation improved the speed of estimation of the primary branch lengths without affecting its accuracy due to the reduced number of points (removing irrelevant points in estimating the primary branch lengths). The skeleton of the whole individual apple tree was also synthesized based on three skeletons of the PB, TK, and EPB, as shown in Fig. 7(d).

2.4.2. Determination of primary branch paths

Each point of the EPB was used to search for the corresponding branch path. Firstly, a final point was determined, which was the point with the minimum depth among all points within the 20 cm lower part of the trunk skeleton, as shown in Fig. 8(a). Then, neighborhood points of each point of skeleton of the whole individual apple tree were quickly retrieved using KD-tree searching algorithm with a radius of 0.05 m (Bentley, 1975). This value of searching radius was set to guarantee to continue searching when encountering gaps in the point clouds. The path from each point of EPB to the final point was searched by iteratively adding points closer to the final point. Searching process would be terminated until the last point on the primary branch path belonged to trunk skeleton or there was no point closer to the final point that can be found within the searching radius, as shown in Fig. 8(b). In the latter case, a point on the trunk skeleton, which was the closest to and lower than the previous last point on the primary branch path, was added to the path as a new last point to ensure connectivity between each primary branch path and the trunk. In other words, the last point of each primary branch path came from the trunk skeleton.

2.4.3. Distinguishing each primary branch instance

A method with three steps (S1, S2, and S3) was developed in this study to distinguish each primary branch instance by merging these paths belonging to the same primary branch, as shown in Fig. 9.

S1: Firstly, paths with fewer than 5 points were deleted. This

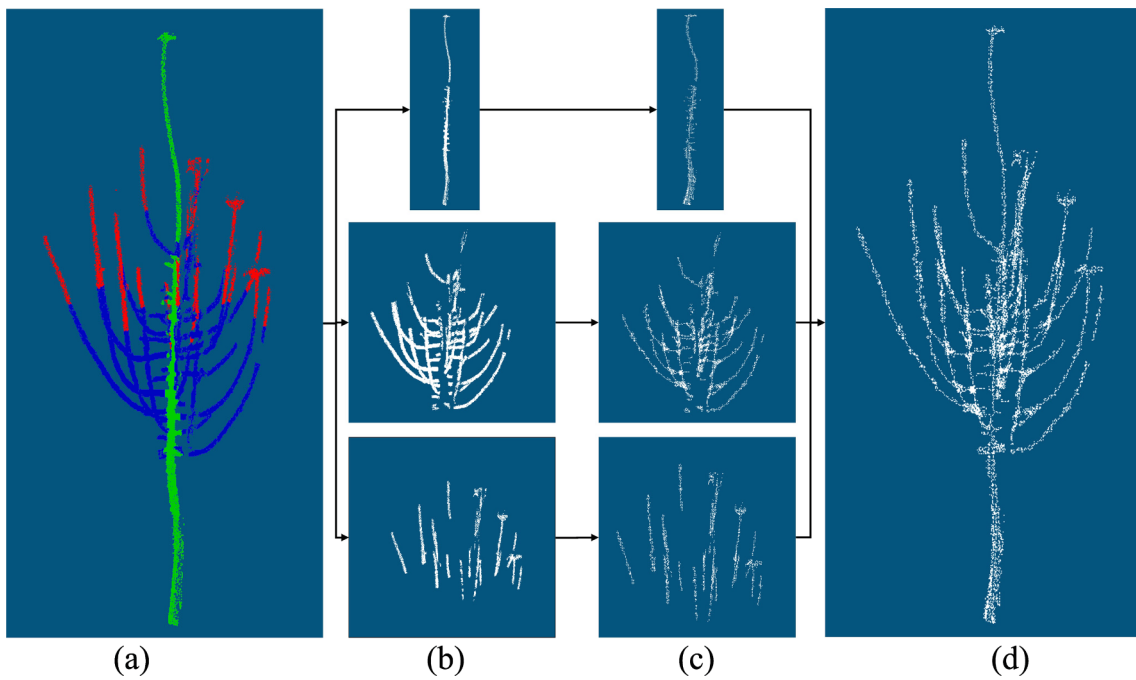


Fig. 7. Skeletonization process of point cloud of an individual apple tree. A test point cloud colored according to the predicted labels (a). Points (b) and skeletons (c) of the PB, TK, and EPB. Skeleton of the whole individual apple tree (d).

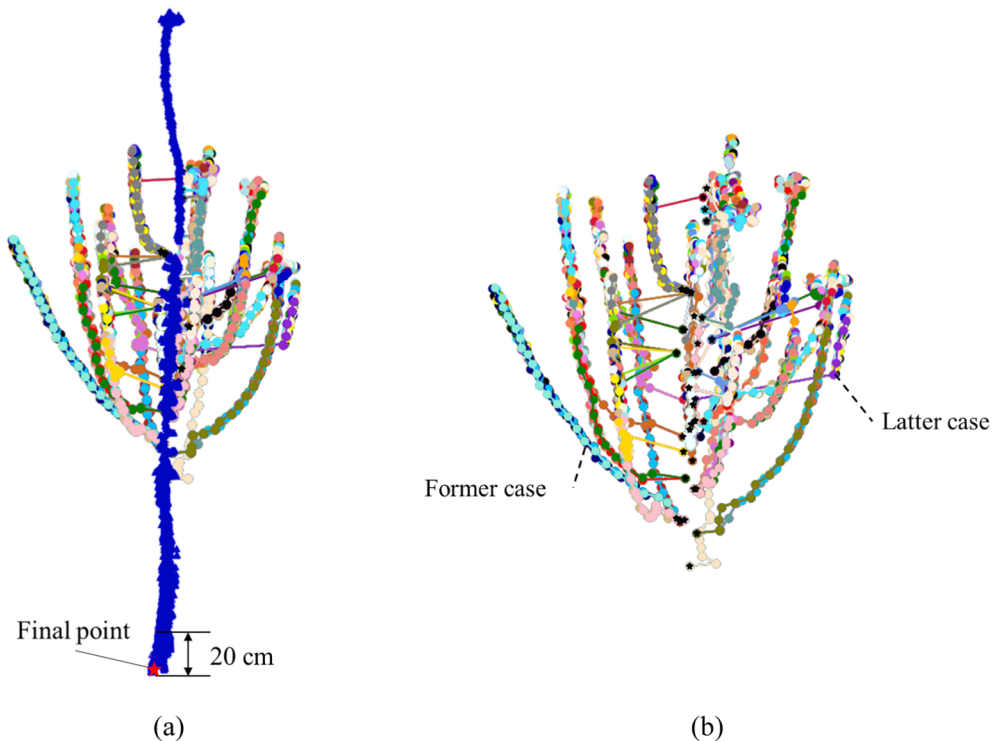


Fig. 8. Example of determining final point that is marked with a red pentagram (a). Each primary branch path was determined (b). The last point on each primary branch path was the trunk skeleton point, which is marked with a black pentagram.

threshold was determined by the minimum length of primary branch, as shown in Fig. 10(b).

S2: Then, any pair of paths with a distance between their starting points less than 0.15 m were merged by removing the short path and retaining the long path, as shown in Fig. 10(c).

S3: Finally, any pair of paths with an average pairwise distance of their corresponding last five points less than 0.05 m were merged by

removing the short path and retaining the long path, as shown in Fig. 10(d).

The remaining primary branch paths were regarded as primary branch instances. Each primary branch instance was used to estimate its length by calculating the sum of Euclidean distances between all adjacent points on the path.

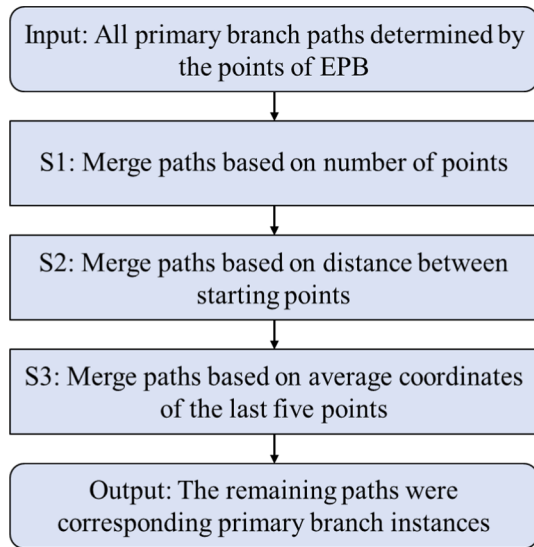


Fig. 9. Flowchart of merging paths to distinguish each primary branch instance.

2.5. Performance evaluation

Overall accuracy (OA), class average accuracy (CAA), and mean *IoU* (*mIoU*) were adopted to evaluate the performance of the trained PointNet++ model for segmenting the PB, TK, and EPB of individual apple trees. They are defined in Eq. (1), Eq. (2), and Eq. (3), respectively.

$$OA = \frac{\sum_{j=1}^m TP_j}{\sum_{j=1}^m N_j} \quad (1)$$

$$CAA = \frac{1}{m} \sum_{j=1}^m \frac{TP_j}{N_j} \quad (2)$$

$$mIoU = \frac{1}{m} \sum_{j=1}^m \frac{|P_j \cap L_j|}{|P_j \cup L_j|} \quad (3)$$

where m is the number of classes. And TP_j (True Positives) represents number of correctly predicted points in class j while N_j represents number of all points of this class. And P_j is the set of points predicted as belonging to class j while L_j is the set of points of class j .

The Performance of the proposed method for estimating primary branch lengths in this study was evaluated by success rate (SR) and mean absolute percentage error (MAPE). SR is the proportion of the estimated number of primary branches to the corresponding ground truth. MAPE is

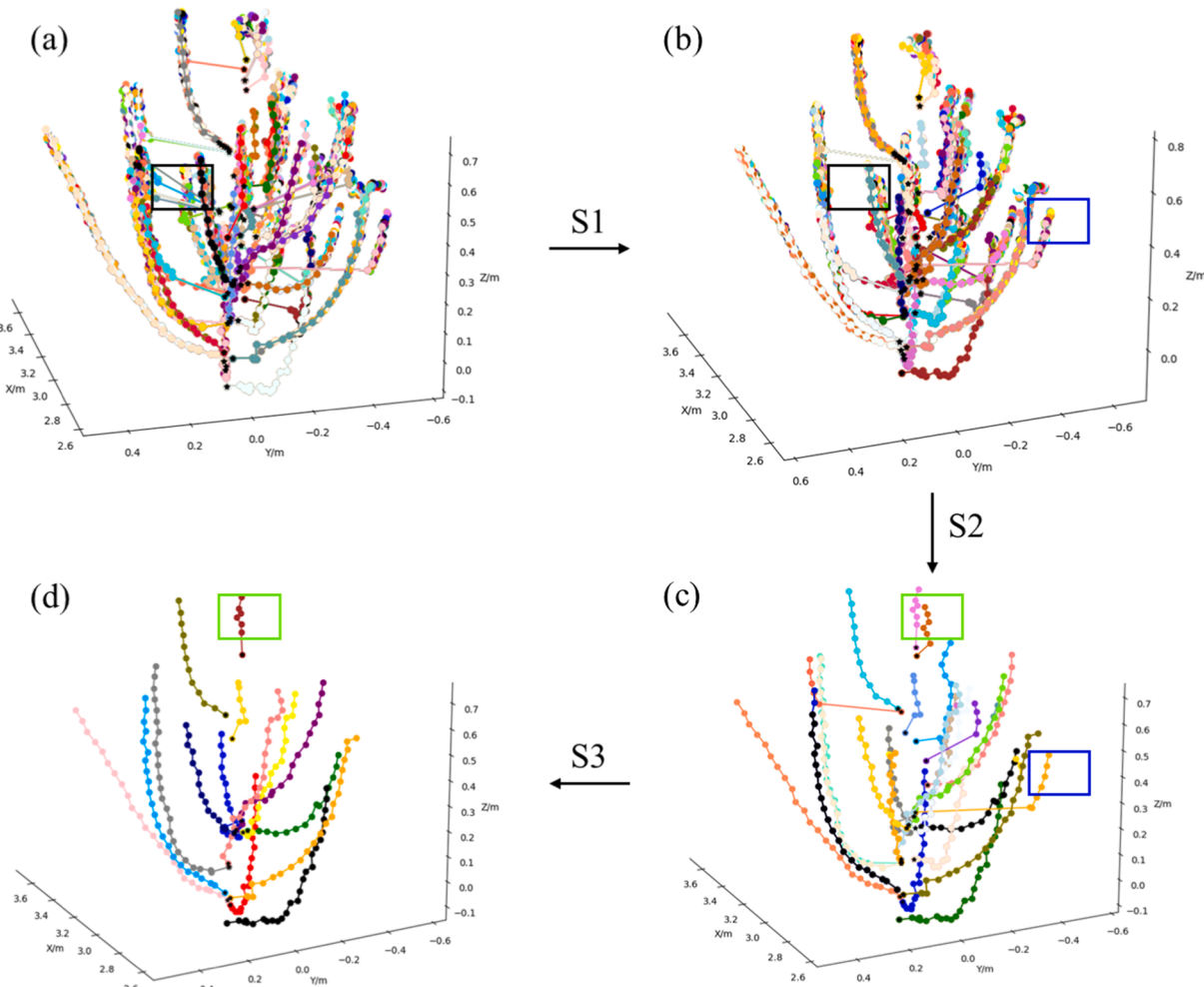


Fig. 10. Primary branch paths were determined (a). Merging primary branch paths belonging to the same primary branch based on number of points (b), distance between starting points (c), and average coordinates of the last five points (d). Examples of removing some primary branches sequentially in three steps are shown in black, blue, and green rectangular boxes, respectively.

a measure of the average error between estimated and ground-truth values of the primary branch lengths. SR and MAPE are calculated by Eq. (4) and Eq. (5), respectively.

$$SR = \frac{N_s}{N_a} \times 100\% \quad (4)$$

$$MAPE = \frac{1}{n} \sum_{k=1}^n \sqrt{\left(\frac{e_k - g_k}{g_k} \right)^2} \times 100\% \quad (5)$$

where N_s and N_a are the number of primary branches that had estimated lengths and ground truth, respectively. And n is the number of samples to estimate the primary branch length. And e_k is the estimated value of the k^{th} primary branch length while g_k is the corresponding ground truth.

Mean absolute error (MAE) was adopted to evaluate performance of estimating the number of primary branches. It is calculated by Eq. (6).

$$MAE = \frac{1}{37} \sum_{p=1}^{37} \sqrt{(N_{ep} - N_{gp})^2} \quad (6)$$

where N_{ep} is the estimated number of primary branches while N_{gp} is the number of primary branches for the p^{th} individual apple tree.

3. Results and discussion

3.1. Performance of PWC and PNC

Training processes of PWC and PNC were effective. As shown in Fig. 11, both OA and $mIoU$ increased and gradually converged as epochs increased. Two models were convergent around the epoch of 250. It showed that both PWC and PNC were able to extract features of the PB, TK, and EPB. They both enabled subsequent segmentation of the three parts of individual apple trees.

3.1.2. Comparison of PWC and PNC

PNC had slightly better performance in segmenting the PB, TK, and EPB, as shown in Table 1. The OA, CAA, and $mIoU$ of PWC reached 0.82, 0.81, and 0.67, respectively, while PNC reached 0.84, 0.83, and 0.70, respectively. The segmentation accuracy of PNC was slightly higher than that of PWC. It indicated that adding color information to train the PointNet++ model could not improve its part segmentation accuracy. The PNC model yielded higher segmentation accuracy than the PWC

Table 1
Segmentation accuracy of PWC and PNC.

Model	OA	CAA	$mIoU$
PWC	0.82	0.81	0.67
PNC	0.84	0.83	0.70

model. Therefore, the PNC model was employed for the part segmentation of point clouds.

Part segmentation outputs of PNC provided a basis for subsequent estimation of the primary branch lengths. Examples of part segmentation outputs of PWC and PNC are shown in Fig. 12. It is evident that PNC had fewer confusions between PB and TK, and obtained higher OA, CAA, and $mIoU$ than those with PWC. The $mIoU$ of PNC reached 0.70 while Liu et al. (2021) employed PointNet to segment branches and leaves of North American crabapple trees with a $mIoU$ of 0.48. Therefore, PNC was utilized to segment the PB, TK, and EPB of individual apple trees in this study.

Adding color information did not improve the segmentation accuracy of PB, TK, and EPB due to their similar color features. Contrary to the results reported by Zhang et al. (2021b), PNC was slightly better than PWC. It may be due to the similarity in color between the TK and PB of apple trees while the objects studied in Zhang et al. (2021b) displayed significant color differences. Our findings are consistent with similar research of Majeed et al. (2018), where they also observed errors in segmenting branches and trunks of apple trees with similar color features.

3.2. Evaluation of estimating number and lengths of primary branches

In this study, the proposed method exhibited potential in estimating the number of primary branches. The relationship between estimated and ground-truth values of the number of primary branches is shown in Fig. 13. There is a strong relationship between estimated and ground-truth values of the number of primary branches. R^2 and MAE reached 0.81 and 1.89, respectively. Sun et al. (2021) employed DBSCAN to count the number of branch instances without leaves on a single cotton plant after pruning parts of branches that were far away from main stalk with average R^2 of 0.70. Similarly, Ma et al. (2021) employed DBSCAN to estimate the number of dormant jujube tree branches without leaves, which gained a R^2 of 0.83 with multi-perspective point clouds collected on sunny days. Comparing with study of Ma et al. (2021), the R^2 of this study was slightly lower because point clouds of individual apple trees collected (for this study) from a single perspective were complex and

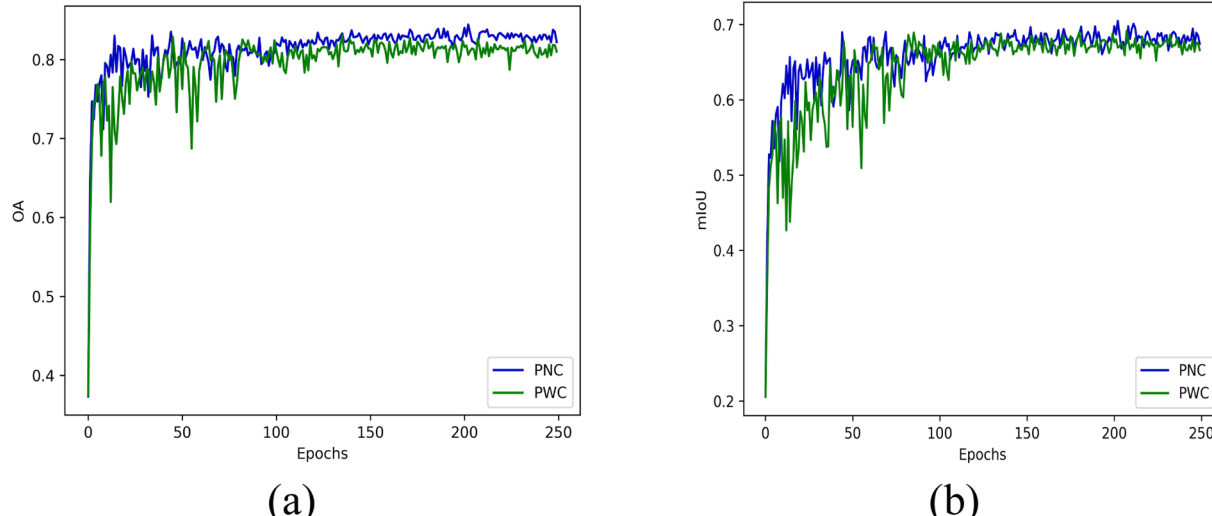


Fig. 11. Curves of OA (a) and $mIoU$ (b) of PWC and PNC.

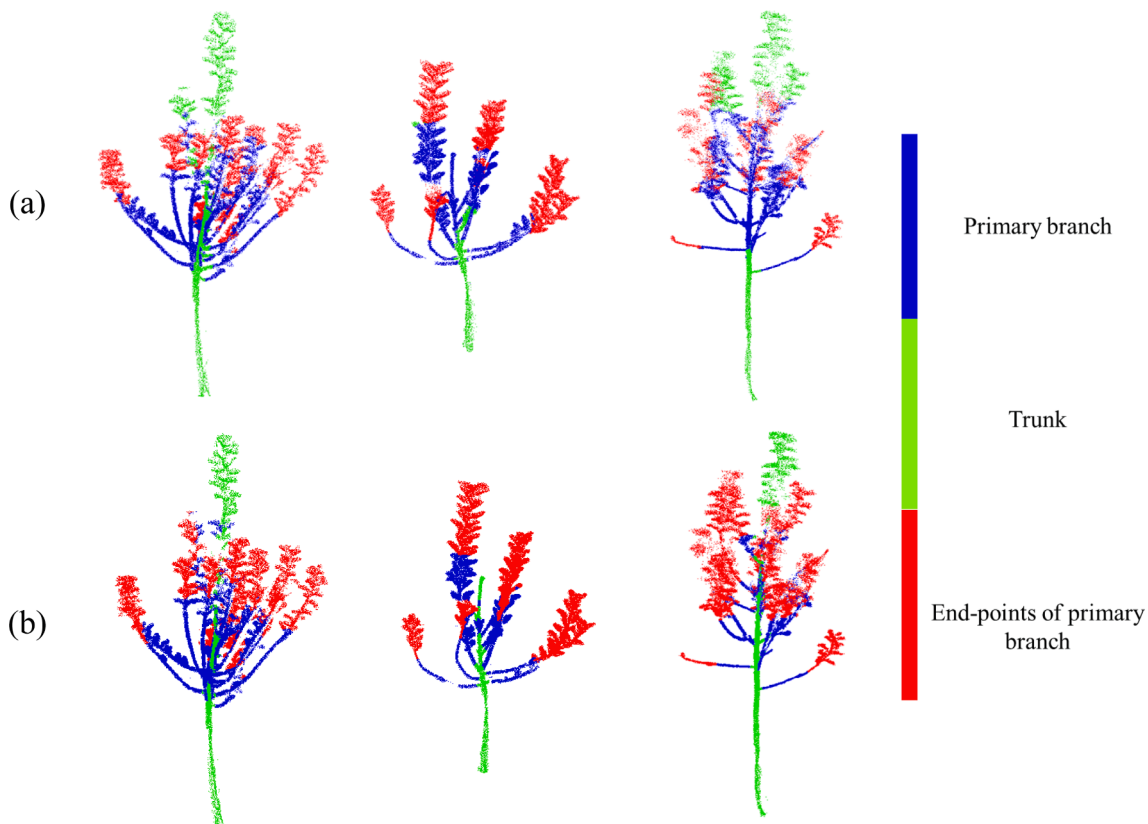


Fig. 12. Examples of part segmentation outputs of PWC (a) and PNC (b).

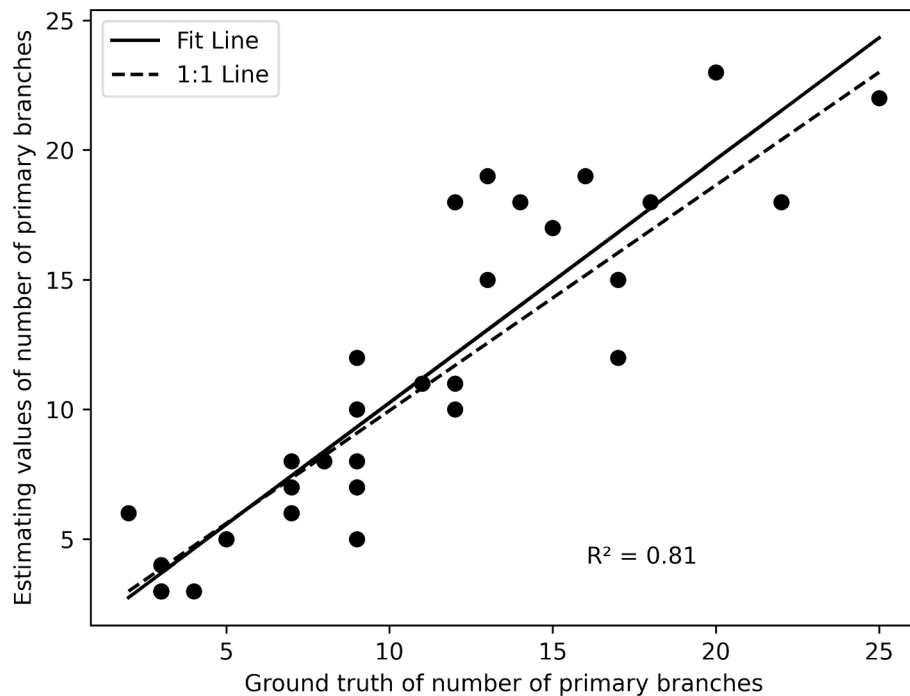


Fig. 13. Relationship between estimated and ground-truth values of the number of primary branches.

occluded. The novel method proposed in this study was able to process point clouds of individual apple trees with some leaves robustly for estimating the number of primary branches.

Method of estimating the primary branch lengths in this study reached a good performance. A strong relationship was established

between estimated and ground-truth values of the primary branch lengths ($R^2 = 0.80$), as shown in Fig. 14. The R^2 of the primary branch lengths in this study was higher than that of 0.77 obtained by Gao et al. (2022). Gao et al. (2022) estimated branch lengths of Korean pine trees indirectly with a branch length model by considering tree attributes and

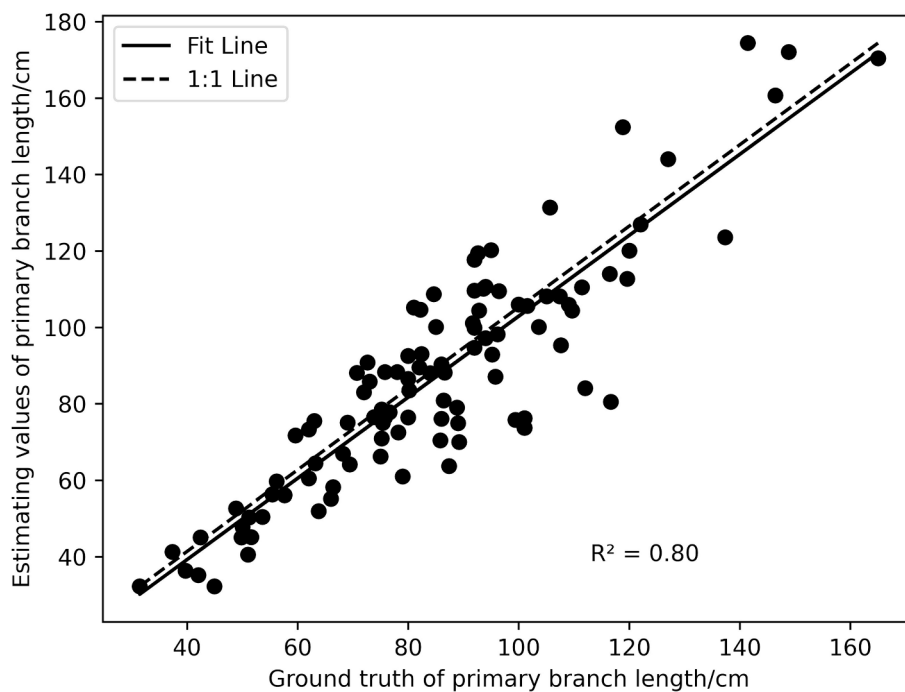


Fig. 14. Relationship between estimated and ground-truth values of primary branch lengths.

competition variables, rather than estimating it directly from point clouds. In their study, *SR* and *MAPE* reached 93.64 % and 12.00 %, respectively. Tabb and Medeiros (2017) proposed a robotic vision system for autonomously sensing and describing the architecture of leafless apple trees against a solid color background, which obtained a mean square error of 4.56 cm for estimating the primary branch lengths. Compared with the study of Tabb and Medeiros (2017), the method proposed in this study had good robustness against point clouds collected in the field. Such point clouds often contained gaps resulting from occluded primary branches and leaves. Hence, it showed potential for estimating the primary branch length of individual apple trees during the deciduous period. In addition, other traits of primary branches, such as diameters and angles to the trunk, need to be further studied.

4. Conclusions

A novel phenotyping method of estimating the primary branch lengths of individual apple trees during the deciduous period was proposed in this study. The primary branch instances were distinguished their instances based on part segmentation outputs obtained by PointNet++. Colored point clouds were employed to train PWC while colorless point clouds were used to train PNC. Comparing the segmentation accuracy of PWC and PNC, it was demonstrated that adding color information did not improve the segmentation accuracy of PB, TK, and EPB, which possessed similar color features. Therefore, PNC was employed to segment the PB, TK, and EPB of individual apple trees. The *OA*, *CAA*, and *mIoU* reached 0.84, 0.83, and 0.70, respectively. Each primary branch instance was distinguished based on the outputs of PNC. Herein the use of deep learning for estimating individual apple tree phenotypes was confirmed. Finally, morphological estimation of the primary branch length was carried out. The method reached a *SR* of 93.64 % and a *MAPE* of 12.00 %. Additionally, the number of primary branches was also estimated with a *MAE* of 1.89. The method proposed in this study demonstrates great potential for estimating the primary branch lengths of individual apple trees during the deciduous period. Moreover, this study extends the period for estimating individual apple tree phenotypes from the dormant period to the deciduous period. These findings contribute to the promotion of high-throughput phenotyping of

individual apple trees during the deciduous period.

CRediT authorship contribution statement

Xiaoming Sun: Writing – original draft, Methodology, Investigation, Data curation. **Leilei He:** Writing – review & editing, Methodology, Investigation. **Hanhui Jiang:** Writing – review & editing, Methodology. **Rui Li:** Writing – review & editing, Supervision, Methodology. **Wulan Mao:** Writing – review & editing, Methodology. **Dong Zhang:** Writing – review & editing, Methodology. **Yaqoob Majeed:** Writing – review & editing, Methodology. **Nikita Andriyanov:** Writing – review & editing, Methodology. **Vladimir Soloviev:** Writing – review & editing, Methodology. **Longsheng Fu:** Writing – review & editing, Supervision, Methodology, Data curation, Conceptualization.

Declaration of competing interest

The authors declare that they have no known competing financial interests or personal relationships that could have appeared to influence the work reported in this paper.

Data availability

Data will be made available on request.

Acknowledgements

This work was supported by the National Natural Science Foundation of China (32171897); Science and Technology Program of Yulin City, China (2023-CXY-183); Open Project of Key Laboratory of Agricultural Equipment for Hilly and Mountainous Areas in Southeastern China (Co-construction by Ministry and Province), Ministry of Agriculture and Rural Affairs, China (QSKF2023002); National Foreign Expert Project, Ministry of Science and Technology, China (DL2022172003L, QN2022172006L).

References

- Abdel-Sattar, M., Kotb, H.R.M., 2021. Nutritional status and productivity of Anna apple trees in the year following autumn irrigation detriment. *Agric. Water Manag.* 252, 106882 <https://doi.org/10.1016/j.agwat.2021.106882>.
- Akbar, S.A., Elfify, N.M., Kak, A., 2016. A novel framework for modeling dormant apple trees using single depth image for robotic pruning application. In: IEEE Int. Conf. Robot. Autom. 5136–5142. <https://doi.org/10.1109/IROS.2016.7487718>.
- Akter, M., Niknejad, N., Bao, Y., Puhl, R.B., Kitt, P., Zheng, J., 2021. Phenotyping of pine tree architecture with stereo vision and deep learning. In: ASABE Annu. Int. Meet. 2100847 <https://doi.org/10.13031/aim.202100847>.
- Bentley, J.L., 1975. Multidimensional binary search trees used for associative searching. *Commun. ACM* 18, 509–517. <https://doi.org/10.1145/361002.361007>.
- Borrenpohl, D., Karkee, M., 2023. Automated pruning decisions in dormant sweet cherry canopies using instance segmentation. *Comput. Electron. Agric.* 207, 107716. <https://doi.org/10.1016/j.compag.2023.107716>.
- Bucksch, A., Fleck, S., 2011. Automated detection of branch dimensions in woody skeletons of fruit tree canopies. *Photogramm. Eng. Remote Sens.* 77 (3), 229–240. <https://doi.org/10.14358/PERS.77.3.229>.
- Chen, Z., Ting, D., Newbury, R., Chen, C., 2021. Semantic segmentation for partially occluded apple trees based on deep learning. *Comput. Electron. Agric.* 181, 105952 <https://doi.org/10.1016/j.compag.2020.105952>.
- Fan, G., Nan, L., Chen, F., Dong, Y., Wang, Z., Li, H., Chen, D., 2020. A new quantitative approach to tree attributes estimation based on LiDAR point clouds. *Remote Sens.* 12 (11), 1779. <https://doi.org/10.3390/rs12111779>.
- Feng, Q., Cheng, W., Li, Y., Wang, B., Chen, L., 2022. Method for identifying tomato plants pruning point using Mask R-CNN. *Trans. Chin. Soc. Agric. Eng.* 38 (3), 128–135. <https://doi.org/10.11975/j.issn.1002-6819.2022.03.015>.
- Gao, H., Liu, Q., Song, Y., Jiang, M., Yin, Y., 2022. Modeling primary branch diameter and length for planted pinus koraiensis by incorporating neighbor competition in northeast China. *Forests* 13, 912. <https://doi.org/10.3390/f13060912>.
- Itakura, K., Miyatani, S., Hosoi, F., 2022. Estimating tree structural parameters via automatic tree segmentation from LiDAR point cloud data. *IEEE J. Sel. Top. Appl. Earth Obs. Remote Sens.* 15, 555–564. <https://doi.org/10.1109/JSTARS.2021.3135491>.
- Jiang, H., Sun, X., Fang, W., Fu, L., Li, R., Cheein, F.A., Majeed, Y., 2023. Thin wire segmentation and reconstruction based on a novel image overlap-partitioning and stitching algorithm in apple fruiting wall architecture for robotic picking. *Comput. Electron. Agric.* 209, 107840 <https://doi.org/10.1016/j.compag.2023.107840>.
- Kok, E., Wang, X., Chen, C., 2023. Obscured tree branches segmentation and 3D reconstruction using deep learning and geometrical constraints. *Comput. Electron. Agric.* 210, 107884 <https://doi.org/10.1016/j.compag.2023.107884>.
- Lee, T.C., Kashyap, R.L., Chu, C.N., 1994. Building skeleton models via 3-D medial surface axis thinning algorithms. *CVGIP Graphical Models Image Process.* 56 (6), 462–478. <https://doi.org/10.1006/cgip.1994.1042>.
- Liang, X., Zhang, X., Wang, Y., 2022. Recognition method for the pruning points of tomato lateral branches using improved Mask R-CNN. *Trans. Chin. Soc. Agric. Eng.* 38 (23), 112–121. <https://doi.org/10.11975/j.issn.1002-6819.2022.23.012>.
- Liu, X., Jing, X., Jiang, H., Younas, S., Wei, R., Dang, H., Wu, Z., Fu, L., 2024. Performance evaluation of newly released cameras for fruit detection and localization in complex kiwifruit orchard environments. *J. Field Robot.* 22297 <https://doi.org/10.1002/rob.22297>.
- Liu, R., Ren, L., Wang, F., 2021. 3D point cloud of single tree branches and leaves semantic segmentation based on modified PointNet network. *J. Phys. Conf. Ser.* 012026 <https://doi.org/10.1088/1742-6596/2074/1/012026>.
- Liu, K., Wang, C., Chen, B., Wang, R., Zeng, J., 2023. Branch development in monoculture and mixed-species plantations of betula alnoidea, erythrophleum fordii and pinus kesiya var. langbianian in southwestern China. *For. Ecol. Manage.* 528, 120643 <https://doi.org/10.1016/j.foreco.2022.120643>.
- Ma, B., Du, J., Wang, L., Jiang, H., Zhou, M., 2021. Automatic branch detection of jujube trees based on 3D reconstruction for dormant pruning using the deep learning-based method. *Comput. Electron. Agric.* 190, 106484 <https://doi.org/10.1016/j.compag.2021.106484>.
- Majeed, Y., Zhang, J., Zhang, X., Fu, L., Karkee, M., Zhang, Q., Whiting, M.D., 2018. Apple tree trunk and branch segmentation for automatic trellis training using convolutional neural network based semantic segmentation. *IFAC-PapersOnLine* 51, 75–80. <https://doi.org/10.1016/j.ifacol.2018.08.064>.
- Miao, Z., Widagdo, F.R.A., Dong, L., Li, F., 2021. Prediction of branch growth using quantile regression and mixed-effects models: An example with planted larix olgensis henry trees in northeast China. *For. Ecol. Manage.* 496, 119407 <https://doi.org/10.1016/j.foreco.2021.119407>.
- Qi, C., Yi, L., Su, H., Guibas, L.J., 2017. PointNet++: Deep hierarchical feature learning on point sets in a metric space. In: Adv. Neural Inf. Proces. Syst. pp. 5100–5109.
- Qiu, T., Cheng, L., Jiang, Y., 2022. 3D characterization of tree architecture for apple crop load estimation. In: ASABE Annu. Int. Meet. 2201119 <https://doi.org/10.13031/aim.202201119>.
- Straub, J., Reiser, D., Lüling, N., Stana, A., Griepentrog, H.W., 2022. Approach for graph-based individual branch modelling of meadow orchard trees with 3D point clouds. *Precis. Agric.* 23 (6), 1967–1982. <https://doi.org/10.1007/s11119-022-09964-6>.
- Sun, X., Fang, W., Gao, C., Fu, L., Majeed, Y., Liu, X., Gao, F., Yang, R., Li, R., 2022. Remote estimation of grafted apple tree trunk diameter in modern orchard with RGB and point cloud based on SOLov2. *Comput. Electron. Agric.* 199, 107209 <https://doi.org/10.1016/j.compag.2022.107209>.
- Sun, S., Li, C., Chee, P.W., Paterson, A.H., Meng, C., Zhang, J., Ma, P., Robertson, J.S., Adhikari, J., 2021. High resolution 3D terrestrial LiDAR for cotton plant main stalk and node detection. *Comput. Electron. Agric.* 187, 106276 <https://doi.org/10.1016/j.compag.2021.106276>.
- Suo, R., Fu, L., He, L., Li, G., Majeed, Y., Liu, X., Zhao, G., Yang, R., Li, R., 2022. A novel labeling strategy to improve apple seedling segmentation using BlendMask for online grading. *Comput. Electron. Agric.* 201, 107333 <https://doi.org/10.1016/j.compag.2022.107333>.
- Tabb, A., Medeiros, H., 2017. A robotic vision system to measure tree traits. In: IEEE Int. Conf. Intell. Robot. Syst. 6005–6012. <https://doi.org/10.1109/IROS.2017.8206497>.
- Tong, S., Yue, Y., Li, W., Wang, Y., Kang, F., Feng, C., 2022. Branch identification and junction points location for apple trees based on deep learning. *Remote Sens.* 14, 4495. <https://doi.org/10.3390/rs14184495>.
- Wang, L., Chen, T., Anklam, C., Goldluecke, B., 2020. High dimensional frustum PointNet for 3D object detection from camera, LiDAR, and radar. In: IEEE Intell. Veh. Symp. pp. 1621–1628. 10.1109/IV47402.2020.9304655.
- Wang, L., Meng, L., Kang, R., Liu, B., Gu, S., Zhang, Z., Meng, F., Ming, A., 2022a. Design and dynamic locomotion control of quadruped robot with perception-less terrain adaptation. *Cyborg. Bionic. Syst.* 9816495 <https://doi.org/10.34133/2022/9816495>.
- Wang, L., Zheng, L., Wang, M., 2022b. 3D point cloud instance segmentation of lettuce based on PartNet. In: IEEE Comput. Soc. Conf. Comput. vis. Pattern Recognit. Workshops 1646–1654. <https://doi.org/10.1109/CVPRW56347.2022.00171>.
- Wu, J., Yang, G., Yang, H., Zhu, Y., Li, Z., Lei, L., Zhao, C., 2020. Extracting apple tree crown information from remote imagery using deep learning. *Comput. Electron. Agric.* 174, 105504 <https://doi.org/10.1016/j.compag.2020.105504>.
- Wu, B., Zheng, G., Chen, Y., Yu, D., 2021. Assessing inclination angles of tree branches from terrestrial laser scan data using a skeleton extraction method. *Int. J. Appl. Earth Obs. Geoinf.* 104, 102589 <https://doi.org/10.1016/j.jag.2021.102589>.
- Yang, C., Wang, Z., Xiong, L., Liu, Y., Kang, X., Zhao, W., 2019. Identification and reconstruction of citrus branches under complex background based on Mask R-CNN. *Trans. Chin. Soc. Agric. Mach.* 50(8), 22–30+69. 10.6041/j.issn.1000-1298.2019.08.003.
- Zahid, A., He, L., Choi, D., Schupp, J., Heinemann, P., 2021. Investigation of branch accessibility with a robotic pruner for pruning apple trees. *Trans. ASABE* 64 (5), 1459–1474. <https://doi.org/10.13031/trans.14132>.
- Zhang, Z., 1999. Flexible camera calibration by viewing a plane from unknown orientations. In: Proc. IEEE Int. Conf. Comput. vis. 666–673. <https://doi.org/10.1109/iccv.1999.791289>.
- Zhang, X., He, L., Majeed, Y., Whiting, M.D., Karkee, M., Zhang, Q., 2018. A precision pruning strategy for improving efficiency of vibratory mechanical harvesting of apples. *Trans. ASABE* 61 (5), 1565–1576. <https://doi.org/10.13031/trans.12825>.
- Zhang, X., He, L., Zhang, J., Whiting, M.D., Karkee, M., Zhang, Q., 2020. Determination of key canopy parameters for mass mechanical apple harvesting using supervised machine learning and principal component analysis (PCA). *Biosyst. Eng.* 193, 247–263. <https://doi.org/10.1016/j.biosystemseng.2020.03.006>.
- Zhang, X., Karkee, M., Zhang, Q., Whiting, M.D., 2021a. Computer vision-based tree trunk and branch identification and shaking points detection in dense-foliage canopy for automated harvesting of apples. *J. Field Rob.* 38 (3), 476–493. <https://doi.org/10.1002/rob.21998>.
- Zhang, Y., Müller, S., Stephan, B., Gross, H.M., Notni, G., 2021b. Point cloud hand-object segmentation using multimodal imaging with thermal and color data for safe robotic object handover. *Sensors* 21 (16), 5676. <https://doi.org/10.3390/s21165676>.
- Zhang, Y., Wu, J., Yang, H., Zhang, C., Tang, Y., 2023. A hierarchical growth method for extracting 3D phenotypic trait of apple tree branch in edge computing. *Wirel. Networks* 7. <https://doi.org/10.1007/s11276-023-03385-7>.
- Zhao, G., Yang, R., Jing, X., Zhang, H., Wu, Z., Sun, X., Jiang, H., Li, R., Wei, X., Fountas, S., Zhang, H., Fu, L., 2023. Phenotyping of individual apple tree in modern orchard with novel smartphone-based heterogeneous binocular vision and YOLOv5s. *Comput. Electron. Agric.* 209, 107814 <https://doi.org/10.1016/j.compag.2023.107814>.
- Zhou, G., Yan, Y., Wang, D., Chen, Q., 2021. A novel depth and color feature fusion framework for 6D object pose estimation. *IEEE Trans. Multimedia* 23, 1630–1639. <https://doi.org/10.1109/TMM.2020.3001533>.
- Zine-El-Abidine, M., Dutagaci, H., Galopin, G., Rousseau, D., 2021. Assigning apples to individual trees in dense orchards using 3D colour point clouds. *Biosyst. Eng.* 209, 30–52. <https://doi.org/10.1016/j.biosystemseng.2021.06.015>.